PERGAMON

Journal of Structural Geology 25 (2003) 575–589

JOURNAL OF STRUCTURAL GEOLOGY

www.elsevier.com/locate/jstrugeo

Asymmetric boudins as shear sense indicators—an assessment from field data

Ben D. Goscombe[a,*], Cees W. Passchier[b]

[a]*Department of Geology and Geophysics, Adelaide University, Adelaide, S.A. 5005, Australia*
[b]*Institut für Geowissenschaften, Johannes Gutenberg Universität, Becherweg 21, 55099 Mainz, Germany*

Received 22 February 2001; received in revised form 31 October 2001; accepted 1 December 2001

Abstract

Asymmetric boudins are potential but problematic shear sense indicators. They can be divided into two groups, with slip on the inter-boudin surface that is either synthetic (S-slip) or antithetic (A-slip) with respect to bulk shear sense. Since both groups have mirror-image symmetry, independent geometric criteria are needed to distinguish them if they are to be used as shear sense indicators. Investigation of asymmetric boudins in trains parallel to the main foliation from the Kaoko Belt in Namibia and elsewhere indicate that the geometry of both groups is in most cases different. *Shearband boudins* (formed by S-slip) have a long, curved lenticular shape and large relative displacement and synthetic drag on an inter-boudin surface that is gently inclined to the boudin exterior surface. *Domino boudins* (formed by A-slip) have an angular shape, an inter-boudin surface steeply inclined to the boudin exterior surface with small relative displacement and unique antithetic flanking folds instead of synthetic drag. *Gash boudins* are a special type of domino boudin with sigmoidal or forked inter-boudin surfaces; they form mostly as foliation boudinage. In boudin trains that were highly oblique to the attractor eigenvector (usually traced by the main foliation), all asymmetric boudin geometries formed by S-slip. Such foliation-oblique boudin trains can, nevertheless, be employed as a second class of shear sense indicator, as in all cases the boudin train as a whole must verge in the same direction as bulk shear sense.

Keywords: Asymmetric boudins; Shear sense; Inter-boudin surface; Synthetic; Antithetic

1. Introduction

Asymmetric boudins, first described in detail by Cloos (1947), Rast (1956) and Uemura (1965) are strips of rock with a rectangular or lozenge-shaped cross-section, separated at regular intervals by interboudin surfaces in the form of veins, fractures or small shear bands. The boudins are arranged in a planar zone, the boudin train, but have usually been displaced with respect to each other along the interboudin surfaces (Fig. 1). Asymmetric boudins are common in high strain zones and shear zones and are amongst the few potential shear sense indicators that are widely developed, of a size useful in the field and which form across a wide range of rock-types, metamorphic grade, bulk strain and flow regimes (e.g. Hanmer, 1986; Gaudemer and Taponnier, 1987; Malavieille, 1987; Marcoux et al., 1987; Goldstein, 1988; Malavieille and Lacassin, 1988; Hanmer and Passchier, 1991). In many medium- to high-grade metamorphic rocks and low-strain terranes they are the only potential shear sense indicators available.

In a section normal to the long axis of individual boudin blocks, asymmetric boudins can be classified according to the two possible senses of slip-direction on the surface separating boudins, compared with bulk shear sense (Swanson, 1992). These are *synthetic slip* (S-slip) *boudinage* and *antithetic slip* (A-slip) *boudinage*, which are mirror images of each other (Fig. 1a). This implies that in order to use asymmetric boudins as shear sense indicators, their S-slip- or A-slip-nature needs to be somehow established, after which bulk shear sense can be determined (Fig. 1a). Several authors have worked on this problem, but no suitable all-encompassing model has yet emerged (Etchecopar, 1974, 1977; Hanmer, 1984, 1986; Simpson, 1984; Malavieille, 1987; Goldstein, 1988; Waldron et al., 1988; Goscombe, 1991; Mandal and Khan, 1991; Swanson, 1992; McNicoll and Brown, 1995).

One possible method to establish slip-sense vergence, investigated in this paper, is to see if the 'kinematic' groups of antithetic- and synthetic-slip boudinage have characteristic geometric features, which could be used to subdivide

* Corresponding author. Tel.: +61-8-8339-1504; fax: +61-8-8339-5758.
E-mail addresses: ben.goscombe@adelaide.edu.au (B.D. Goscombe), cpasschi@mail.uni-mainz.de (C.W. Passchier).

0191-8141/03/$ - see front matter © 2002 Elsevier Science Ltd. All rights reserved.
PII: S0191-8141(02)00045-7

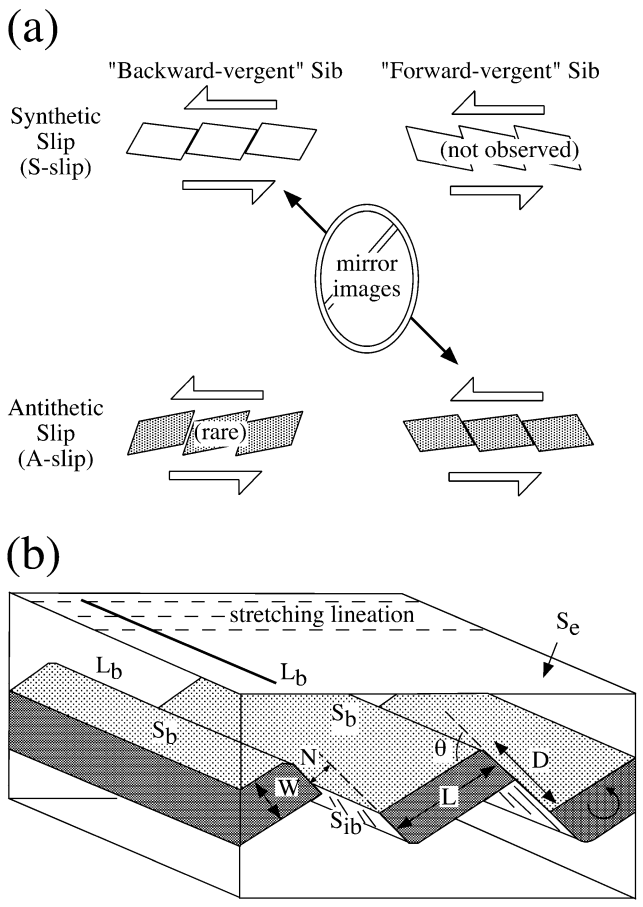

Fig. 1. (a) Asymmetric boudinage is defined either by a deviation of the boudin shape from a rectangle, expressed as forward or backward vergence of the inter-boudin surface; or by the slip-sense on the inter-boudin surface, compared with bulk shear sense in the host rock. Four possible categories of asymmetric boudins are defined in this way, of which one is never observed, and a second one is rare. The two remaining cases are each other's mirror image, and therefore need other, independent geometric criteria to be distinguished in the field. (b) Nomenclature and symbols used for boudin structural elements and geometric parameters in asymmetric boudin structures. Explanation in text.

boudin structures into corresponding geometric classes. If this could be established, the *geometry* of boudins could be used in the field to predict whether they formed by S-slip or A-slip boudinage, and they could then be used as independent shear sense indicators.

Features characteristic of boudin geometric classes can be found by experimental or numerical studies and this has been attempted to some extent (Hanmer, 1986; Goldstein, 1988; Mandal and Karmakar, 1989; Mandal and Khan, 1991). However, the number of parameters that can influence the geometry of developing boudins is so great as to be a serious limitation to experimental and theoretical work. We therefore decided to investigate the range of possible geometries of natural boudins in relation to bulk shear sense, where the latter is known by independent means. To this end, we determined the geometry and kinematics of a large number of natural boudin structures to see if they can be grouped into geometric classes defined by shape parameters that are easily identifiable in the field. Our examples are mainly from the Neoproterozoic Kaoko Belt in Namibia, augmented from other areas and from the literature. The appendix briefly describes the geology of the Kaoko Belt as a background to this study. We measured geometric parameters and recorded qualitative features for 995 boudins either directly in the field, or on photographs. A summary of the data is given in Table 1.

2. Geometric parameters of boudins

We use the term inter-boudin surface (S_{ib}) to indicate either a discrete slip-surface separating boudins, or an imaginary 'skeletal' median surface through the centre of a matrix- or mineral-filled inter-boudin gap or thinned boudin neck (Fig. 1b). S_{ib} does not propagate beyond the boudinaged layer (in contrast to faults) and usually swings into and terminates parallel to the enveloping surface (S_e) of the boudinaged layer at the edge of individual boudin blocks. If individual boudin blocks (strips) have been displaced relative to another along S_{ib}, this leads to 'block rotation', i.e. the orientation of the boudin exterior (S_b), the outer surface of the individual boudin blocks, will differ from the enveloping surface (S_e) of the boudinaged layer, also known as the boudin train (Fig. 1b). In this study, boudins with block rotation $>5°$ are treated as asymmetric boudins. A linear feature L_b is defined by the long axis, edge or neck-zone of the boudin (Fig. 1b).

S_{ib} and L_b are commonly highly oblique or normal to a stretching or mineral lineation (Fig. 1b). Most boudins investigated have monoclinic symmetry and we therefore restrict our study to 2D-geometry in the *profile plane*, normal to L_b. In the profile plane, boudin asymmetry can have two types of vergence compared with bulk shear sense (Fig. 1a). These can be defined by (1) the sense of slip on S_{ib} (A-slip, S-slip) or the sense of block rotation with respect to S_e and; (2) the inclination of S_{ib} with respect to S_b being either forward-vergent or backward-vergent (Fig. 1b) in the same sense as 'backward-tilted' and 'forward-tilted' of Swanson (1992).

The geometry of asymmetric boudins can be uniquely described in the profile plane by the following minimum number of parameters (Fig. 1b); (1) length (L) measured parallel to S_b; (2) width (W) measured normal to S_b; (3) relative displacement (D) between individual boudins measured parallel to S_{ib} and normal to L_b; (4) dilation of S_{ib} (N) measured normal to S_{ib} and (5) the angle θ ($0 \geqslant \theta \geqslant 90°$) between S_{ib} and S_b.

Another important aspect besides the geometry and mutual arrangement of individual boudins is the orientation of the boudin train with respect to the main foliation in the rock matrix. The foliation may be approximately parallel to the boudin train (foliation-parallel boudin trains) or oblique (foliation-oblique boudin trains). We found that 96% of

Table 1
Mean values of parameters and diagnostic features of boudins in both foliation-parallel and foliation-oblique boudin trains

	Foliation-parallel boudin trains			Foliation-oblique boudin trains	
	Domino boudins		Shearband boudins	Domino boudins	Shearband boudins
	Normal domino	Gash			
Number of observed boudins	399	56	310	191	39
Boudin shape and nature					
Inter-boudin surface (S_{ib})	Sharp, straight	Sharp, sigmoidal or forked	Ductile/sharp, sigmoidal/straight	Sharp plane	Sharp/ductile
S_{ib}–S_e relationship	S_{ib} terminates as S_e	S_{ib} discordant to S_e	S_{ib} terminates as S_e	S_{ib} curves into S_e	S_{ib} curves into S_e
Boudin shape	Angular rhomb	Angular rhomb to sigma lens	Sigma lens or rhomb	Angular rhomb	Angular rhomb to sigma lens
Associated kinkbands	None	None	Rare	None	None
Inter-boudin zone fill	Host (68%), vein (32%)	Vein (75%), host (25%)	Host (96%), vein (4%)	Vein (60%), host (40%)	Host (100%)
Foliation boudinage	3.5%	94.6%	0.0%	0.0%	0.0%
Boudinage with respect to tectonic transport					
Slip on S_{ib}	A-slip (100%)	A-slip (100%)	S-slip (100%)	S-slip (100%)	S-slip (100%)
S_{ib} inclination vergence	Forward (100%)	Forward (91%)	Backward (100%)	Forward (100%)	Backward (100%)
Flanking fold on S_{ib}	42%	62%	0%	6%	0%
Synthetic drag on S_{ib}	13%	0%	98%	0%	100%
No deflection on S_{ib}	45%	38%	2%	94%	0%
D_3–D_4 episode of boudinage[a]	9.9%	5.0%	11.3%	0%	40%
Angular and dimensional parameters (mean)					
θ-block shape	71.5°	81.8°	39.3°	77.6°	47.2°
L/*W* (aspect ratio)	2.12	1.39	3.62	3.48	3.22
D/*W* (normalised displacement)	0.47	0.08	2.25	0.38	1.52
% with displacement on S_{ib}	100%	73%	100%	99%	100%
N/*L* (S_{ib} dilation, if present)	0.17	0.05	0.02	0.1	–
% with dilation across S_{ib}	24%	77%	2%	48.5%	0%
Stretch (extension of S_e)	123%	105%	160%	113%	138%
% with isolated boudins	15%	0%	58%	26%	62%

[a] Data from Kaoko Belt only. Brackets indicate proportion of data in indicated category.

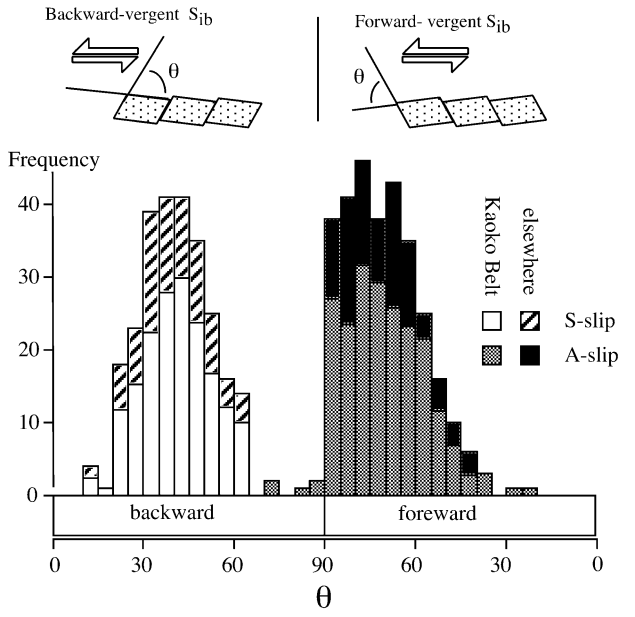

Fig. 2. Histogram showing the frequency of observed boudins in foliation-parallel boudin trains for specific values of θ, the angle between the inter-boudin surface S_{ib} and the boudin exterior, S_b. θ shows either forward or backward vergence with respect to bulk shear sense. At $\theta = 90°$, boudins with backward- and forward-vergent S_{ib} have the same geometry and therefore the horizontal axis represents a continuous gradient of all possible orientations of S_{ib}. Boudins with S-slip and A-slip are separated in the diagram. 540 boudins from the Kaoko Belt, 172 boudins from elsewhere and from the literature. Further explanation in text.

boudins in the Kaoko Belt are foliation-parallel boudin trains. It is these foliation-parallel boudin trains that are described in the next paragraphs, unless stated otherwise.

3. Methodology

All boudins from the Kaoko Belt were measured in profile section, orthogonal to the long axis of the boudins. Throughout the area investigated, only sinistral strike-slip shear sense has been found (Appendix A; Fig. A1) but nevertheless, care was taken that at each locality shear sense was determined independently, based on mantled porphyroclasts of σ-type and δ-type (Passchier and Simpson, 1986), C′- and C-type shear band cleavages (Berthé et al., 1979; Platt and Vissers, 1980; Passchier and Trouw, 1996) and flanking folds (Hudleston, 1989; Passchier, 2001).

As a first approach, we expressed boudin geometry in foliation-parallel boudin trains by the minimum number of normalised parameters that fully describe boudin-outline (as explained above), i.e. *L*/*W*, *D*/*W*, *N*/*L*, and θ. Fig. 2 shows the frequency of θ for boudins with monoclinic symmetry, with synthetic (S-slip) or antithetic slip (A-slip) on S_{ib} and forward- or backward-vergent S_{ib} (Fig. 1a) as determined from independent shear sense indicators. We found that boudins with S- and A-slip are clearly separated without an overlap. S-slip boudins all have backward-vergent S_{ib} with θ of 10–65°. A-slip boudins have backward-vergent S_{ib} from 70 to 90° or forward-vergent S_{ib} from 20 to 90° (Fig. 2). This applies not only for 540 boudins from the Kaoko Belt, but also for 172 additional ones where bulk shear sense has been independently determined, observed elsewhere in the field or obtained from the literature (Fig. 2). Although this separation is an interesting result, it is unfortunately not of much direct use to field geologists since shear sense, and therefore the forward- or backward-vergent nature of S_{ib}, *cannot* be determined independently in most field situations. We therefore plotted all measured data in diagrams of θ against normalised boudin parameters where we neglect the forward or backward-vergent nature of boudins, to see if there is still some separation of the fields of S- and A-slip. This is the case for diagrams of θ against *D*/*W*, *L*/*W* and *N*/*L* (Fig. 3). The advantage of these plots is that they spread out the measurements and so allow investigation of a possible relationship between the boudin parameters and slip type.

Two populations are apparent in each combination plot in Fig. 3: those containing more than 98% S-slip boudins, more than 98% A-slip boudins and a zone of overlap containing both. S-slip boudins dominantly have low θ values and none plot at angles over 64° while A-slip boudins have $\theta > 41°$ (Fig. 3a–c). *D*/*W* and *N*/*L* have a relationship with boudin slip type. All A-slip boudins have small relative displacement (*D*/*W* values <1.8) and S-slip boudins show higher relative displacement mostly exceeding 1.8 (Fig. 3a). S-slip coincides with very low or no dilation across S_{ib} (*N*/*L*), while A-slip coincides more commonly with some dilation of S_{ib}. The identified domains and trends discussed above apply not only to the boudins observed in the Kaoko Belt, but also to the 172 boudins from other locations (Fig. 3). Nevertheless, it may be dangerous to try and predict the S-slip or A-slip nature of asymmetric boudins from the size of *D*/*W*, *N*/*L* and θ alone. We therefore tried to characterise the geometry of boudins in the dominant (98%) S-slip and dominant (98%) A-slip domains in Fig. 3 more precisely based on our observations in the Kaoko Belt and elsewhere, spanning a wide range in flow regimes, strain, metamorphic grade and rock-types.

4. Geometry of asymmetric boudins

4.1. Introduction

Careful investigation of the boudins in our data set from the dominant S-slip and dominant A-slip domains of Fig. 3 show that boudins in each group not only differ by the main shape parameters, but also by a large number of minor structural features that may prove crucial for their recognition (Fig. 4). In order to separate the kinematic description (S-slip, A-slip) from purely geometrical descriptions (not associated with boudin development mechanisms) we use separate names for these two categories. In the literature, a number of names have been proposed for asymmetric

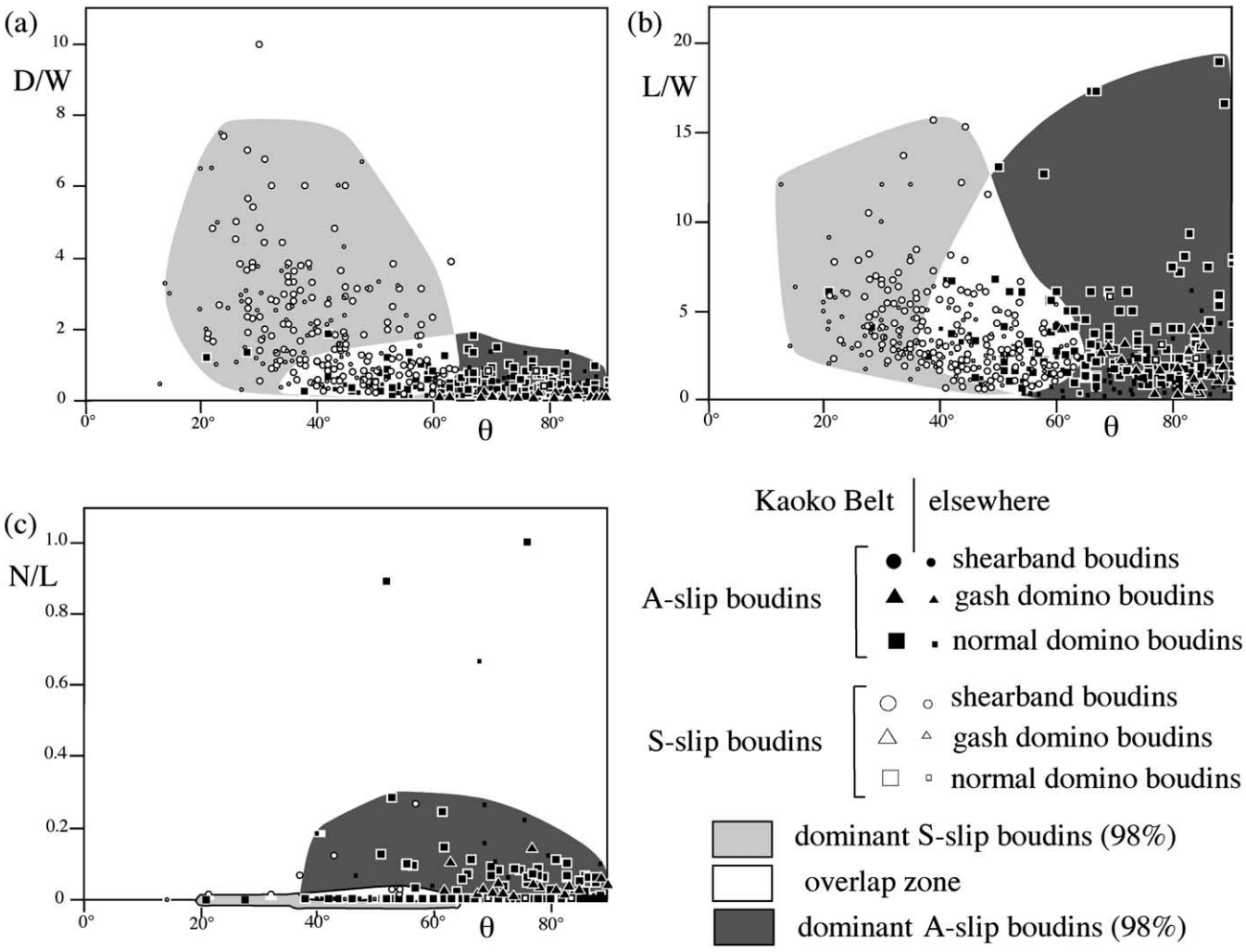

Fig. 3. Measurement plots of the main parameters that describe boudin geometry from our data set of foliation-parallel boudin trains. Open symbols indicate S-slip; closed symbols A-slip. A subdivision can be made based on the dominant presence (>98%) of A-slip and S-slip boudins, indicated by shading. The closed and open symbols have been differentiated to show the distribution of S-slip and A-slip over the geometric types of boudins. Large symbols indicate measurements from the Kaoko Belt; small symbols measurements from elsewhere. (a) $D/W-\theta$ plot; (b) $L/W-\theta$ plot; (c) $N/L-\theta$ plot. 540 boudins from the Kaoko Belt, 172 boudins from elsewhere and from the literature. Further discussion in the text.

boudins. For those in the dominant S-slip domain these are; shear fracture boudinage (Mandal and Khan, 1991; Swanson, 1992; Mandal et al., 2000); Type III boudinage (Goldstein, 1988); Type 2B pull-aparts (Hanmer, 1986); asymmetric extension boudinage (Gaudemer and Tapponnier, 1987); antithetically rotated asymmetric pull-aparts (Jordan, 1991) and counter-rotating boudinage (Grasemann and Stüwe, 2001). For those in the dominant A-slip domain earlier proposed names are: domino- or bookshelf structure (Etchecopar, 1977); Type 1 asymmetric pull-aparts (Hanmer, 1986); forward rotated extension fracture boudinage (Swanson, 1992) and co-rotating boudinage (Grasemann and Stüwe, 2001).

Many of these names are either not strictly geometric, or may cause confusion with other systems in structural geology. We therefore propose to call structures as found in the dominant S-slip domains of Fig. 3 *shearband boudins* and those found in the dominant A-slip domains of Fig. 3 *domino boudins*; the typical geometry of each type is described in the next sections.

4.2. Shearband boudins

Shearband boudins (Fig. 4a; name inspired by Swanson (1992)) have the following properties. Boudin blocks have an asymmetric, rhomb to lens-shape similar to that of σ-type mantled porphyroclasts (Passchier and Simpson, 1986; Goldstein, 1988); shapes with tapering wings are typical (Figs. 4a and 5a–c). S_{ib} is typically a discrete surface in the field, mostly recognisable in thin section as a thin (<1 mm) ductile shear zone with associated ductile grain-refinement and a grain-shape fabric. In some cases S_{ib} constitutes a wider ductile zone. The obtuse edge of the boudin is commonly rounded and the acute edge is drawn into a tapering wing by drag on S_{ib}. S_{ib} is straight to curvi-planar (Fig. 5c) and at a low angle to S_b (θ averaging 39°) (Figs. 3 and 5a–c). Aspect ratios of the

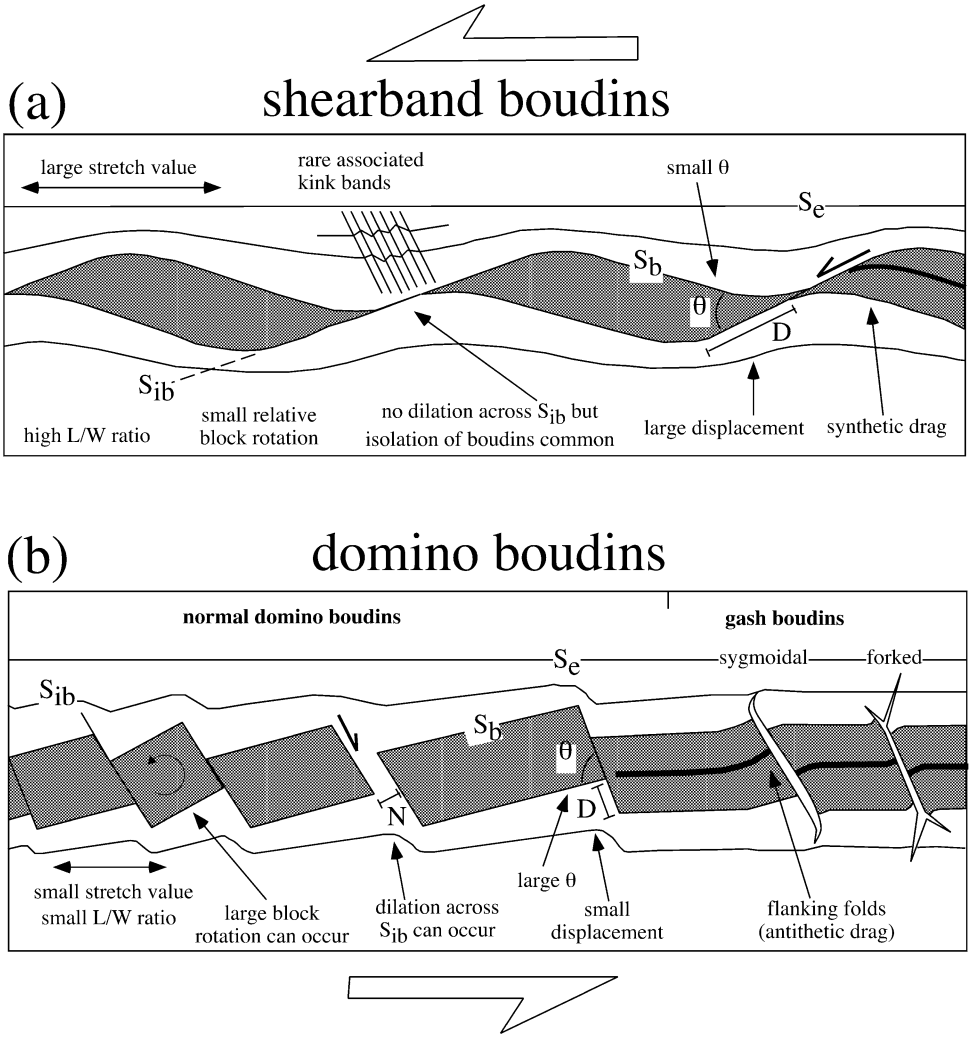

Fig. 4. Sketch illustrating the salient features of (a) shearband boudins and (b) domino boudins, based on average angular and dimensional parameters and annotated with the most diagnostic features.

boudin blocks are high, *L*/*W* averaging 3.6 (Table 1; Fig. 5a). Dilation across S_{ib} and vein-infill is very rare and where present is very small (Table 1). Lateral displacement on S_{ib} is the highest of all boudin-types, *D*/*W* averaging 2.25. Consequently, extension of S_e is high and results in complete isolation of adjacent boudin blocks in more than half of the investigated cases (Table 1). Shearband boudins have antithetic block rotation with respect to shear sense in all investigated cases and all have backward-vergent S_{ib} (Table 1). The degree of relative block rotation is typically lower than for domino boudins, but this is not diagnostic (Table 1). Synthetic drag on S_{ib} is evident in nearly all cases (Table 1). This is a diagnostic feature of shearband boudins and is responsible for the typical, tapering shapes of the boudin block. In some cases, kink bands are associated with shearband boudins (cf. Gaudemer and Taponnier, 1987), but never with other types of asymmetric boudins. These kink bands have a wavelength of 2–5 mm and axes parallel to L_b, and occur in the inter-boudin zone in the domain of flattening immediately adjacent to the boudin surface (S_b) (Fig. 4). Kink band axial surfaces are inclined at a high angle to S_{ib}. Shearband boudins with a geometry as defined above were earlier described in papers by Cloos (1947), Ramberg (1955), Malavieille (1987), Marcoux et al. (1987), Malavieille and Ritz (1989) and Stock (1989).

4.3. Domino boudins

Domino boudins are named after Etchecopar (1977) for a resemblance with tumbling domino stones (Figs. 4b and 6), although the similarity is lost when boudins have high *L*/*W* ratio. In most cases S_{ib} is a discrete, sharp surface except where there has been dilation across S_{ib}, resulting in two parallel terminal faces either side of the inter-boudin zone. Domino boudins have rhomb shapes with low aspect ratio (*L*/*W* averaging 2.1; Table 1), typically with angular boudin edges and sharp, straight to rarely curvi-planar S_{ib} (Fig. 6). S_{ib} is at a high angle to S_b, with θ averaging 72° (Table 1; Fig. 3). Lateral displacement (*D*) along S_{ib} is low (Fig. 3a). Low *D* and high θ imply low extension of the enveloping

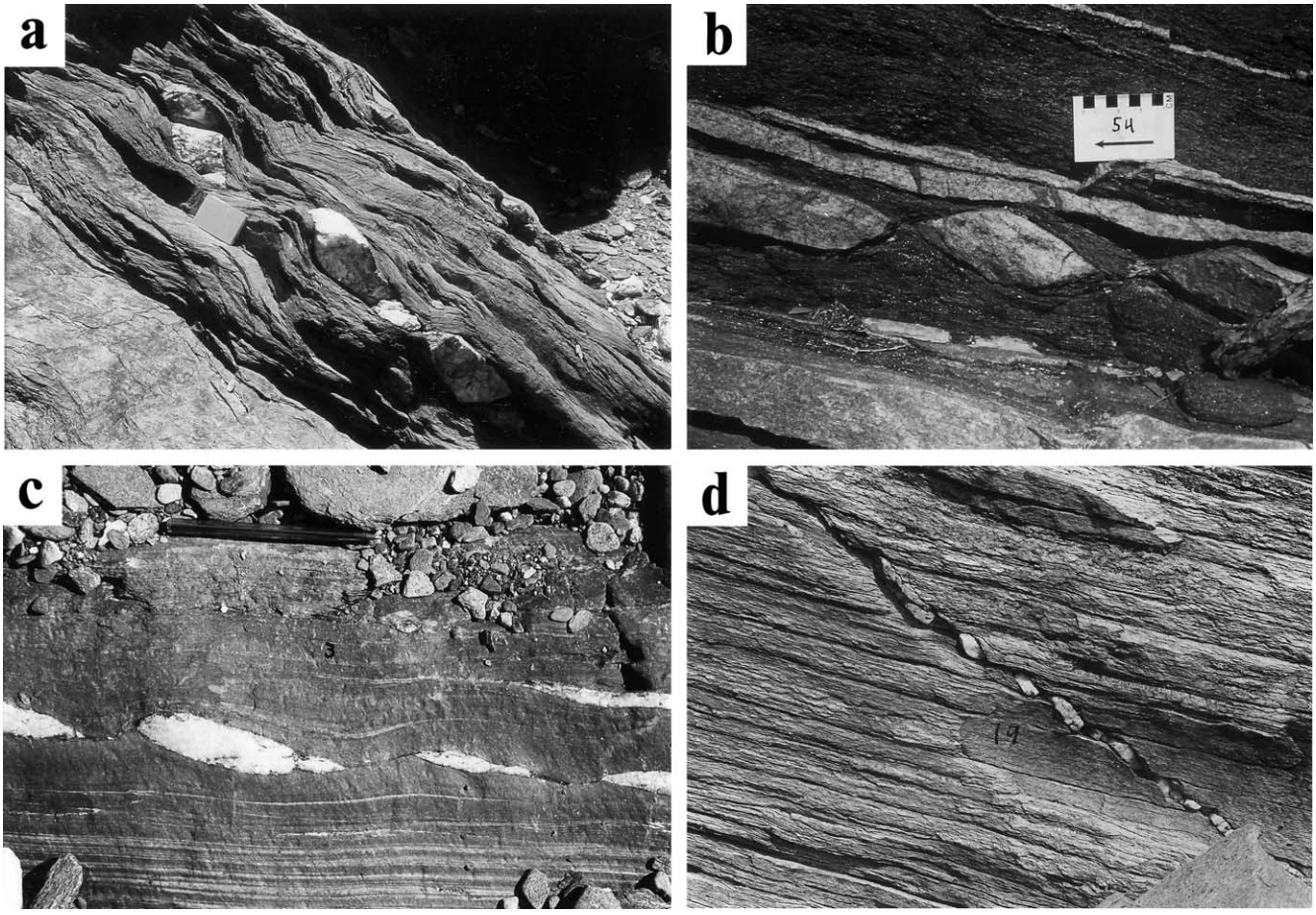

Fig. 5. Photographs of shearband boudins, all with sinistral bulk shear sense. (a) Foliation-parallel train of shearband boudins of quartz-vein in biotite–sericite schist. Note associated kink bands. Notebook for scale. (b) Foliation-parallel train of shearband boudins of quartzo-feldspathic gneiss in schistosic host. (c) Foliation-parallel train of shearband boudins of quartz-vein in meta-greywacke schist. Pencil for scale. (d) Foliation-oblique boudin train of shearband boudins of quartz-vein in quartz–sericite schist. Width of view 50 cm. Note that the boudin geometry with respect to the enveloping surface is similar in both foliation-oblique (d) and foliation-parallel boudin trains (a–c). All photographs from the Kaoko Belt, Namibia.

surface and as a result, complete isolation of boudins is relatively uncommon. In contrast to shearband boudins, dilation across S_{ib}, with or without vein-infill does occur (24% of investigated cases) and is diagnostic. Block rotation is inversely proportional to aspect ratio, with strong rotation of up to 54° occurring only for equant boudins with *L*/*W* near one. In nearly all domino boudins, vergence defined by S_{ib} inclination is forward-vergent, as shown in Fig. 1a.

Where deflection of internal planar structures along S_{ib} is present in boudins, it is antithetic to slip on S_{ib} resulting in *flanking folds* (Figs. 4b and 6b; Hanmer, 1986, fig. 3b; Hudleston, 1989; Swanson, 1992; Grasemann and Stüwe, 2001; Passchier, 2001). Flanking folds occur in 42% of cases and are unique and diagnostic for domino boudins; they were not observed in shearband boudins. The flanking folds probably form in response to internal ductile deformation of the boudins in shear, causing rotation of S_{ib} from an original orthogonal or backward-vergent orientation to the typical forward-vergent orientation of domino boudins (Fig. 7). Following the model of Hudleston (1989), this happens by local flow partitioning in the inter-boudin zone into antithetic slip on S_{ib} and low-vortical flow inside the boudin in a narrow strip along S_{ib}, leading to development of flanking folds when S_{ib} rotates with respect to S_e (Grasemann and Stüwe, 2001; Passchier, 2001). In general, flanking folds occur more frequently and are better developed in domino boudins with a high aspect ratio (*L*/*W*) than in those with a low aspect ratio. Probably, those with low aspect ratio can accommodate external non-coaxial flow in the matrix entirely by block rotation while boudins with high aspect ratio cannot rotate at the same rate and deform internally, leading to development of flanking folds. The half wavelength of flanking folds averages 0.65 of the layer width *W*. Domino boudins of a geometry described above were earlier described by Etchecopar (1977), Mawer (1987), Malavieille (1987), McLellan (1988) and further studied and classified by Hanmer (1986), Malavieille and Lacassin (1988), Waldron et al. (1988) and Swanson (1992).

4.3.1. Gash boudins

Normal domino boudins have a straight unbranched inter-boudin surface or gap, but some are characterised by a

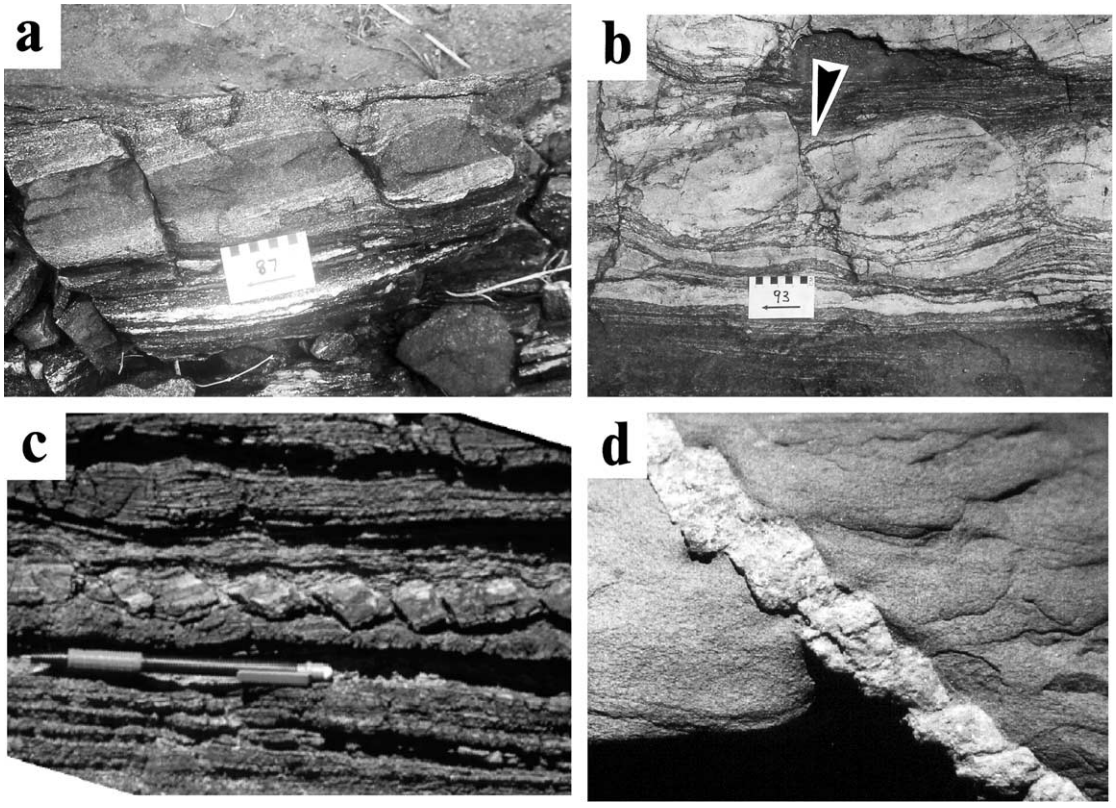

Fig. 6. Photographs of domino boudins, all with sinistral bulk shear sense. (a) Foliation-parallel train of planar domino boudins of mafic layer in quartzo-feldspathic gneiss. Kaoko Belt, Namibia. (b) Typical domino boudins in layered quartzo-feldspathic gneiss with flanking fold indicated. Kaoko Belt, Namibia. (c) Typical blocky domino boudins with low *L*/*W* developed in calc–silicate layers within a carbonate matrix. Arunta Block, Central Australia. (d) Foliation-oblique boudin train of domino boudins blocks in a quartz-feldspar vein in meta-greywacke. Adelaidean Fold Belt, South Australia.

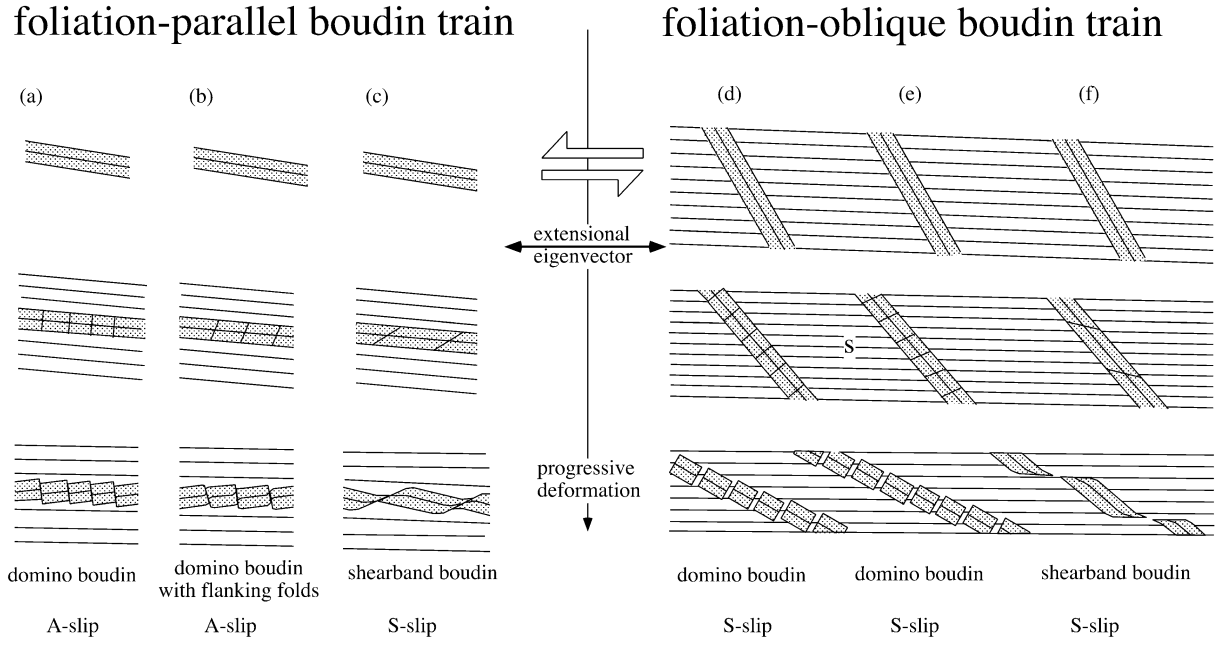

Fig. 7. Schematic presentation of the inferred sequence of development of different types of boudins. (a)–(c) Foliation-parallel boudin trains where a foliation develops parallel to boudin trains during progressive deformation. (a) Original high or orthogonal θ and little internal deformation leads to domino boudins with A-slip. (b) Original high-angle backward-vergent S_{ib} can develop into domino boudins with high θ, A-slip, and flanking folds. (c) Original low-angle backward-vergent S_{ib} leads to development of shearband boudins with S-slip. (d)–(f) Foliation-oblique boudins where an older foliation is cut by a planar body, which is subsequently subject to boudinage. (d) Original high or orthogonal θ and little internal deformation leads to domino boudins, but with S-slip. (e) Original high-angle backward vergent S_{ib} can develop into domino boudins with high θ and S-slip. Flanking folds are rare because of the gentle dip of the S_{ib} with respect to the extensional eigenvector. (f) Original low-angle backward-vergent S_{ib} leads to development of shearband boudins with S-slip.

prominent strongly curved or segmented gash, separating the boudins and are therefore named *gash boudins* (Fig. 4b). These boudins are almost exclusively developed by foliation boudinage (Lacassin, 1988; Swanson, 1992) and can be further subdivided into sigmoidal- and forked-gash boudins (Fig. 4b). Sigmoidal gash boudins (sigmoidal boudin partings of Swanson (1992)) have a smooth sigmoidal S_{ib} trace (Fig. 4b). Forked-gash boudins (reoriented extension fractures of Swanson, 1992) have an angular S_{ib} trace comprised of a straight central section and forked or inclined crack terminations ('Swordtail' and 'Fishmouth' terminations of Swanson (1992)). Forked terminations are asymmetric; the dominant branch (longer and more dilated) is in the opposite direction of bulk shear sense, typically forming the larger acute angle to the central S_{ib} trace (Fig. 4b). In our data set, the S_{ib} trace of both types is not only sigmoidal or angular in the profile plane normal to L_b, but also in the S_e plane of view, indicating a complex three-dimensional form with triclinic symmetry.

The aspect ratio of gash boudins is extremely low, *L*/*W* averaging only 1.39 (Table 1). The length of gash boudins along L_b averages only 1.2 times *L*. Other observed boudin-types mostly extend along L_b at least beyond the scale of the outcrops and their dimension along L_b exceeds *L* by at least a factor of 10. Dilation and associated vein-infill is common in gash boudins (77% of investigated cases), but with very small dilation (Table 1). Small dilation coupled with small displacement on S_{ib} results in very low extension of the enveloping surface (Table 1). Displacement on S_{ib} is recognised in 73% of cases and almost all are A-slip boudins. Displacement with respect to dilation is low compared with all other asymmetric boudins.

Flanking folds are common in the central portion of S_{ib} in 62% of investigated cases, with synthetic drag of the enveloping foliation only evident at the tips of S_{ib}, resulting in the 'kink-band' terminations described by Swanson (1992). Block rotation is low and synthetic to bulk shear sense (Table 1). The central portion of S_{ib} is nearly orthogonal to the boudin exterior (S_b), with θ averaging 82°. Vergence defined by both inclination-direction and sigmoidal shape of S_{ib} is the same in nearly all cases and synthetic with bulk shear sense, that is forward-vergent (Fig. 4b). The degree of curvature of S_{ib}, from the central straight portion to the tips, has a large range of 10–66°, but consistently averages 32° in both the profile and S_e planes of view for gash boudins.

5. Discussion

5.1. Mechanisms of boudinage

Although the aim of this paper is to present field data on the geometry of asymmetric boudins and their relationship to shear sense, the observations may also bear some relevance to the mechanisms by which asymmetric boudins form. The following general scheme can be summarised from the literature, based on experimental work and theoretical considerations.

Boudins can be separated based on the dominant nature of deformation in the boudin neck on the grain scale: brittle, brittle–ductile or ductile. This difference is partly based on metamorphic grade, strain, flow regime and lithology, but may also be influenced by strain rate, pore fluid pressure and the presence and distribution of melt.

Boudinage by brittle fracturing can initiate as tensile fractures initially normal or oblique to layering, or along oblique shear fractures (e.g. Tvergaard et al., 1981; Lloyd et al., 1982; Gaudemer and Taponnier, 1987; Goldstein, 1988; Jordan, 1991; Swanson, 1992; Mandal et al., 2000). The length–width ratio of the resulting boudins decreases with increasing strain by repeated fracturing up to some equilibrium value (Lloyd et al., 1982). Once normal or shear fractures have formed, boudins can start to separate and rotate with respect to S_e to develop the characteristic synthetic or antithetic slip of asymmetric boudins (Fig. 7). The type of asymmetric boudin to form and boudin separation *N* will mostly depend on the initial boudin aspect ratio *L*/*W*, θ and the orientation of the layer with respect to the extensional eigenvectors of flow in the rock (Strömgård, 1973; Goldstein, 1988; Passchier and Druguet, 2002). Other factors of importance are flow parameters such as the kinematic vorticity number (Means et al., 1980; Passchier and Druguet, 2002) and the rheology of layering and matrix. For boudin trains parallel to the extensional flow eigenvector, boudins can accommodate all shear deformation in the matrix by block rotation and deform into domino boudins without flanking folds if θ is high (close to orthogonal) and aspect ratio *L*/*W* is small (Fig. 7a; Goldstein, 1988; Mandal and Karmakar, 1989; Mandal and Khan, 1991); 'rigid' domino boudins of little block rotation can also form if *L*/*W* is high, but if the boudins can deform internally in response to non-coaxial flow in the matrix (simple shear or general flow) the inter-boudin surface rotates with respect to S_e congruent with shear sense and flanking folds develop as outlined above (Fig. 7b; Hudleston, 1989; Swanson, 1992; Grasemann and Stüwe, 2001; Passchier, 2001). The presence of flanking folds illustrates that in many domino boudins, internal ductile deformation was important despite their angular aspect and the fact that the boudins apparently initiated by brittle fracturing.

If the aspect ratio *L*/*W* is high and θ is low and backward-vergent (Swanson, 1992), slip on S_{ib} leads to only minor block rotation, forward or even backward with respect to S_e (Ghosh and Ramberg, 1976; Passchier, 1987; Passchier and Druguet, 2002). Synthetic slip on the interboudin surfaces produces shearband boudins in this case (Fig. 7c). Even if such boudins can deform internally, S_{ib} can only rotate slowly forward, and will in general not rotate at all, or even backward (Swanson, 1992). Therefore, flanking folds will not form. On the other hand, separation is less on shearband boudins than on domino boudins (Swanson, 1992), and therefore synthetic 'drag' in the slip-direction

along S_{ib} will be stronger for shearband- than for domino boudins (Figs. 4 and 7a–c). This may explain why synthetic drag is common in shearband boudins, and flanking folds are common in domino boudins. Flanking folds and synthetic drag may therefore be the most important features for distinguishing between shearband- and domino boudins (cf. Swanson, 1992; Grasemann and Stüwe, 2001).

The scheme outlined above is supported by our observations, as follows. For almost all geometric parameters there is a continuous range from symmetric boudins to domino boudins manifested by an increase in D, in flanking fold half-wavelength and a decrease in θ (Fig. 3). Sense of slip and vergence of S_{ib}, where present, are the same for these boudin-types. The continuous range of geometric parameters suggest that angular symmetric boudins with high θ evolved by block rotation and further stretch to domino boudins with forward-vergent S_{ib}. This is supported by the strong asymmetry of the curve for A-slip boudinage in Fig. 2 with a leading edge at $\theta = 90°$, trailing to lower forward-vergent values. This probably results from an initial orthogonal S_{ib} and subsequent decrease of θ by internal deformation of part of the boudins.

Gash structures can develop in foliation boudinage, evolving from symmetric boudins in the same way as other domino boudins, but with a complex evolution of S_{ib}. Where there is no dilation, the initial crack is 'forward-tilted' to a forked-gash boudin geometry (Lacassin, 1988; Swanson, 1992) or ordinary domino boudin. Where dilation across S_{ib} is present, sigmoidal-gash or dilational domino boudins develop. Sigmoidal-gash boudins form by lateral growth of S_{ib} where it is laterally unconstrained in foliation boudinage (Swanson, 1992). In contrast, lateral growth of S_{ib} is inhibited by layer width in normal domino boudins.

Since drag on S_{ib} is synthetic to slip in shearband boudins, the S_{ib} surface can be regarded as a discrete shear zone of finite length that terminates at the boudin edge, swinging into parallelism with the enveloping surface (S_e). Shearband boudins are analogous to shear band cleavage (C'-type), and in fact the average geometries of both are very similar (Malavieille, 1987; Goldstein, 1988; Swanson, 1992). Where both are developed in the same outcrop, the orientation of both S_{ib} and C' are identical, although C'-cleavage is not necessarily related to a specific layer and is laterally continuous. High D/W indicates that slip on S_{ib} is the dominant mechanism of layer extension in shearband boudin trains.

Although some shearband boudins may develop from brittle fractures (Goldstein, 1988), most probably form by nucleation and growth of minor ductile shear zones or bands of the same sense as bulk shear that develop at a small angle to S_e. Once such shear bands develop in this orientation, they could grow further into shearband boudins. The typically large aspect ratio of shearband boudins may imply that the shear bands nucleate at a relatively large distance from each other, and less frequently than the initial fractures in brittle boudin types.

On the mineral grain-scale, where initiation of S_{ib} is controlled by pre-existing mineral cleavage planes, both shearband- and domino-type structures can form. Where mineral cleavage is at low angles to the extensional flow eigenvector, the result is shearband boudin geometry such as for mica-fish (Lister and Snoke, 1984) or orthopyroxene-fish (Goscombe and Everard, 2001). Mineral grains with less well-developed cleavage planes crack more randomly, commonly at a high angle to the extensional flow eigenvector, resulting in domino boudins in garnet, feldspar and sillimanite grains (Simpson and Schmid, 1983; Simpson, 1984; Goscombe, 1991, 1992; Yamamoto, 1994).

5.2. Foliation-oblique boudin trains

All observations on asymmetric boudins discussed above were made on *foliation-parallel boudin trains*, which apparently experienced the entire deformation history of the rock and developed together with the main foliation. This is typically boudinage of bedding during development of the pervasive layer-parallel foliation. There are also boudin trains, however, which lie oblique to the main foliation in the rock, in some cases up to 60° (Figs. 5d and 6d). This happens, for example, where, during ongoing deformation, a dyke intruded oblique to the already developed foliation and was boudinaged in the last stages of the deformation event (Goldstein, 1988; Hanmer and Passchier, 1991; Jordan, 1991), or where bedding has been rotated by folding into an angle oblique to the extensional flow eigenvector. In the Kaoko Belt, 4% of observed asymmetric boudins are such *foliation-oblique boudin trains*. They have also been observed in other areas, and we have data on a total of 230 foliation-oblique boudin trains (Table 1).

As described above, we found that in foliation-parallel boudin trains, shearband boudins with small θ form by S-slip boudinage, whereas stocky domino- or gash boudins with high θ (near orthogonal) form by A-slip boudinage. Foliation-oblique boudin trains developed in a different way. Asymmetric boudins of either domino- or shearband geometry as shown in Fig. 4 also develop in foliation-oblique boudin trains (Fig. 5d), but *all* 230 foliation-oblique boudin trains investigated formed by S-slip irrespective of their domino-, gash or shearband geometry (Fig. 7; Table 1). Therefore, the distinction of A-slip and S-slip boudins by boudin geometry does not work, apparently, for foliation-oblique boudin trains.

This aberrant behaviour can be explained as follows. Material lines such as boudin trains rotate towards the extensional eigenvector or eigenvectors of bulk flow such as those in the 'flow plane' of simple shear (Ghosh and Ramberg, 1976). Such 'attractor' eigenvectors seem to lie commonly parallel to the shear zone boundary (Passchier, 1997, 1998). If the initial angle between a boudin train and the attractor eigenvector is small, less than 30°, the initial angle θ mainly determines the slip direction on the inter-boudin surface, as discussed above. In this case, the boudin train experiences the entire deformation history and

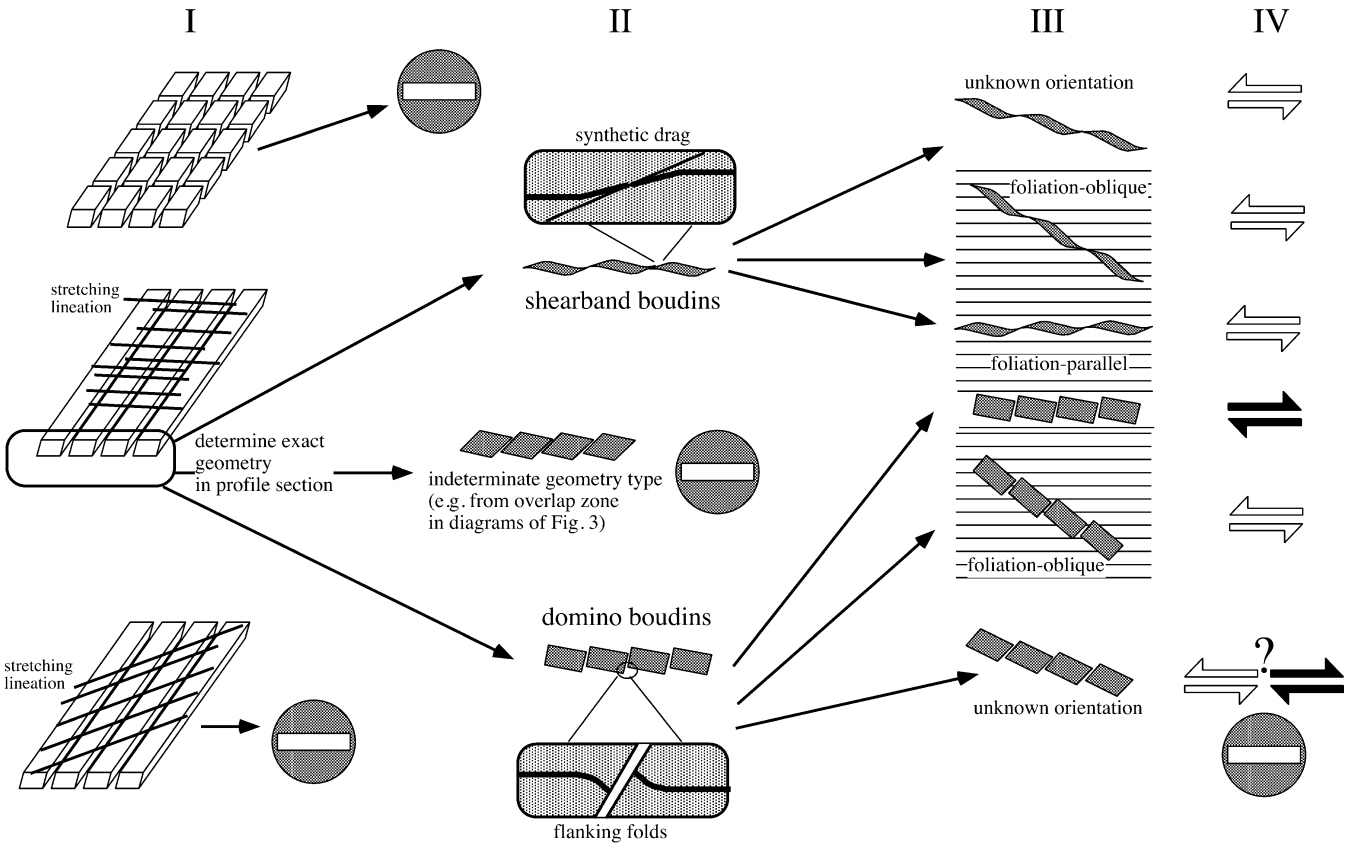

Fig. 8. Proposed procedure to use asymmetric boudins for determining sense of shear. (I) Only boudins with a profile section parallel to the stretching lineation in the rock and strip-shaped boudins are suitable for the analysis. (II) Boudin geometry should be compared with Fig. 4 to determine whether boudins classify as shearband or domino types. In doubt the geometry can be tested against Fig. 3. Any suspect boudins should not be analysed further. (III) In the next step, the foliation-parallel or oblique nature of the boudin trains is considered. (IV) In nearly all cases, boudins can now be used to determine shear sense as shown, except for trains of domino boudins of uncertain orientation with respect to a foliation in the host rock; they cannot be used. Notice that foliation-oblique trains of domino boudins can be used to determine shear sense since the trains must lie in the extensional part of the flow field. Further explanation in the text.

develops into a foliation-parallel boudin train. If, however, the initial angle between a boudin train and the attractor eigenvector is high, e.g. 70°, not only boudins with low θ, but also those with high θ and domino-type geometry will be affected by S-slip boudinage (Fig. 7d–f; Ghosh and Ramberg, 1976; Goldstein, 1988). There will be a "critical initial angle" between attractor eigenvector and boudin train, which depends on flow parameters, boudin shape, mechanical contrasts and probably other factors, where rotation rate of boudins and the boudin train is equal. This critical angle is the boundary between S-slip and A-slip boudinage for all boudins with high θ, such as domino- and gash boudins. By contrast, all boudins with low θ and forward-vergent S_{ib} such as shearband boudins are less sensitive to the angle between the attractor eigenvector and the boudin train, and form by S-slip.

Obviously, the behaviour of foliation-oblique boudin trains diminishes the reliability of employing asymmetric boudin geometry as a shear sense indicator in these boudin trains. However, the situation is not so bad in practice. Although position of the attractor eigenvector of flow cannot normally be found, the final angle between the boudin train and the main foliation in the rock can be taken as a guide (Fig. 8). If the angle is negligible or small, the boudin train probably initiated at a small angle to the attractor eigenvector and rotated into an orientation close to the attractor eigenvector. In this case, the interpretation as foliation-parallel boudin trains is as given in Section 4. If the angle with the foliation is high, asymmetric boudins should be interpreted with more care. High-θ boudins of this type are difficult to interpret while low-θ boudins can be interpreted as S-slip boudins without reserve (Fig. 8). Consequently, if the angle of a boudin train with respect to the foliation is unclear, for example, if no foliation is developed as in many marbles, boudins with shearband geometry may still be reliable shear sense markers, but boudins with domino-geometry are not (Fig. 8).

Despite the difficulties discussed above, the vergence of a foliation-oblique boudin train itself with respect to the attractor eigenvector can be employed as a different type of shear sense indicator, which is independent of the geometry of the boudins (cf. 'oblique boudin trains' in Hanmer and Passchier (1991)). Where it is possible to show that a boudinaged layer did develop at a high angle to the attractor

eigenvector, it must have rotated towards the attractor eigenvector in the direction of bulk shear sense (Fig. 7d–f). This is because, for boudinage to occur in a high-angle layer, the layer must have been forward-vergent towards the attractor eigenvector and contained within the extensional field of the strain ellipsoid (Fig. 7d–f). Any layer that is backward-vergent towards the attractor eigenvector will be shortened and not manifest as a boudin train. This holds for all geometries of boudins developed in the boudin train and for foliation-oblique boudin trains formed in both coaxial and non-coaxial progressive deformation.

6. Evaluation of asymmetric boudins as shear sense indicators

Asymmetric boudins within all foliation-parallel and many foliation-oblique boudin trains can be applied as shear sense indicators if natural boudin structures can be confidently identified as domino- or shearband boudins (Figs. 4 and 8). Despite differences in metamorphic grade, kinematics of deformation and other factors it is usually possible to separate asymmetric boudins into these two geometric classes. There is overlap in individual geometric parameters (Fig. 3), but if a suite of the most diagnostic geometric criteria is considered (Fig. 4), boudins can be classified in most cases. We propose that the most successful attempt to use asymmetric boudins as shear sense markers is in four steps (Fig. 8):

1. Confirm that the boudin axis (L_b) is at high angle to the stretching lineation in the rock. If this is not the case, boudins may have developed in triclinic flow or have been modified by polyphase deformation, and no attempt should be made to use them as shear sense indicators. However, boudin structures can be employed in poly-deformed terranes provided that the boudin structure can be related to fabrics of specific deformation events (Goscombe and Passchier, 2001).
2. Determine whether the boudins correspond to the secondary shape characteristics of shearband- or domino boudins as discussed above and shown in Fig. 4. Shape of the boudin blocks and presence of synthetic drag in shearband boudins versus flanking folds in domino boudins are the most diagnostic and easily recognised criteria. Boudin shape is quantified by θ; most shearband boudins have $\theta < 58°$ and tapering shapes and most domino boudins and all gash boudins have $\theta > 58°$ and angular blocky shapes (Fig. 3). Shearband boudins are also characterised by a higher aspect ratio (L/W), greater displacement along S_{ib} (D) and stretch, commonly resulting in isolated boudin blocks. Dilation across S_{ib} (N) is restricted almost entirely to domino boudins (Fig. 4).
3. Establish whether the boudin trains are foliation-parallel or foliation-oblique (Fig. 8).
4. (a) In *foliation-parallel boudin trains*, all shearband boudins will be S-slip and most domino boudins will be A-slip. This can be checked by measuring L, D, W, N and θ, and determine where the boudins plot in the diagrams of Fig. 3. If the inferred shearband boudins, or inferred domino- or gash boudins fall in their respective fields out of the field of overlap, they are probably reliable. If they consistently fall in the field of overlap, they must be disregarded. (b) In *foliation-oblique boudin trains*, shearband boudins will be S-slip, but domino types can be either S- or A-slip and boudin block geometry in this case is not a reliable indicator of shear sense (Fig. 8). Regardless of boudin geometry, the vergence of foliation-oblique boudin trains as a whole can be employed as a second class of shear sense indicator, where the boudin train must verge in the same direction as bulk shear sense (Figs. 7 and 8).

A further word of caution should be given here: our data are mostly from one orogenic belt and although we have made an effort to include all asymmetric boudins that we could find, further work might show that the boundaries in Fig. 3 should be shifted, or that other parameters must be included as well.

In our work, we have not made an attempt to subdivide boudins further according to additional parameters such as metamorphic grade, inferred kinematic vorticity number of flow, finite strain intensity, boudin and matrix lithology etc. Such a subdivision could help to decrease the size of the overlap domains in Fig. 3 and make more boudins available for shear sense analysis. However, some of these additional parameters are difficult to establish with confidence and most are difficult to establish in the field. In this work, we therefore restricted ourselves to parameters that can easily be collected in the field.

Acknowledgements

Roy Miller, Rudolph Trouw, Fabio Pentagna, Andre Ribeiro, Chris Wilson, Thomas Bekker, Dave Gray, Elena Druguet, Paul Bons, Pat James, Martin Hand, David and Audrey Goscombe, Helmut Garoeb, Zigi Baugartner, Pete and Alex Siegfried, Murray Haseler and Bonza are all thanked for their discussions, efforts spying out elusive boudins and great company in the field. Martin Hand provided a photograph of domino boudins. This study resulted from regional mapping work undertaken for the Namibian Geological Survey and self-funded fieldwork elsewhere (BG). The fieldwork associated with this study was supported to CWP by the Schürmann Foundation. Mimi Duneski is sincerely thanked for her considerable administrative support and humour in Namibia. Ben Grasemann is thanked for providing us with his manuscript in press.

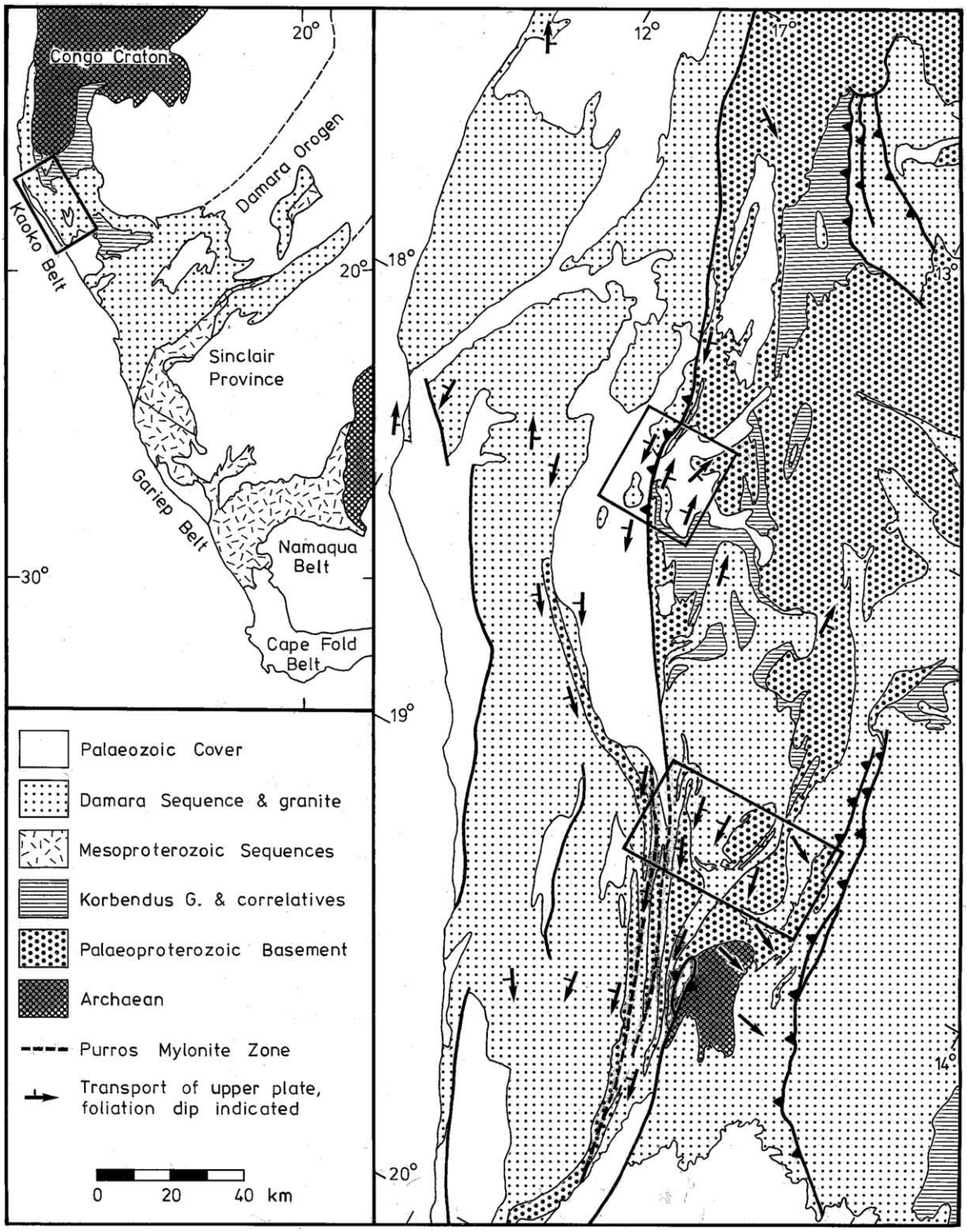

Fig. A1. Schematic geological map of the Kaoko Belt. Areas mapped in detail are outlined and sense of D_2 transport is indicated.

Appendix A

A.1. Geology of the Kaoko Belt

The Kaoko Belt is the northern coastal arm of the Neoproterozoic–Palaeozoic Damara Orogen within Namibia (Fig. A1). The Damara Sequence is comprised of metagreywacke, quartz-mica schists, meta-arenites and metaturbidites with numerous meta-diamictite, amphibolite schist, quartzite and carbonate units. The Damara Sequence rests unconformably on a highly variable basement complex dominated by Palaeoproterozoic quartzo-feldspathic

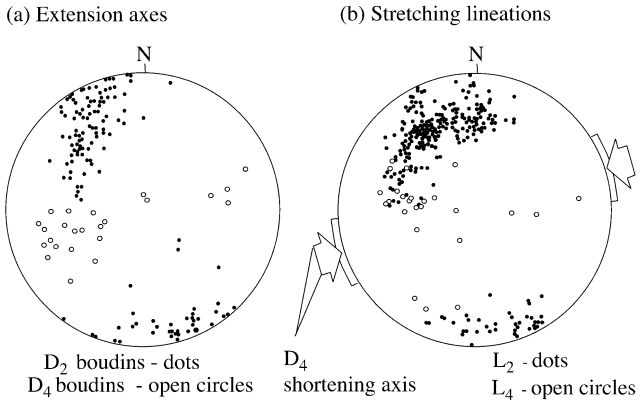

Fig. A2. Lower-hemisphere, equal-angle stereoplots comparing the orientation of D_2 and D_4 boudin extension axes and mineral stretching lineations. (a) Boudin extension axes (L_e). The spread in extension axes is due to a change from D_2–D_3 transpressional movement to E-directed D_4 over-folding; (b) L_2 and L_4 stretching lineations and the average shortening axis during D_4 over-folding.

paragneisses with granitoid orthogneisses of 1970–1977 Ma age, and a terrane containing Archaean orthogneisses of 2585–2645 Ma age (Seth et al., 1998) (Fig. A1). The Kaoko Belt trends NNW–SSE and can be divided into three parallel zones. The East Kaoko Zone, east of the thrust faults in Fig. A1, comprises the sub-greenschist Damara platform sequence dominated by carbonates and resting on the Palaeoproterozoic Kamanjab Inlier. The Central Kaoko Zone is highly deformed and ranges from lower greenschist to upper amphibolite grade in the west. The Western Kaoko Zone, west of the Purros mylonite zone (Fig. A1), is a complex of Damaran granitoids of 656 Ma and 552–580 Ma ages (Kröner, 1982; Miller and Burger, 1983; Seth et al., 1998) and upper-amphibolite to granulite-grade Damara Sequence rocks.

In the basement complexes, one or more pre-Damaran tectono-thermal cycles (collectively described as D_1) are inferred by high-grade early parageneses, gneissic textures, abundant partial melt segregations and Proterozoic granitoids. Reworking during the Damara Orogeny was so intense that pre-Damaran structures are only rarely preserved. The Damara Orogeny involved a single progressive orogenic cycle (D_2–D_4) accompanying peak metamorphism (552–580 Ma). D_2 was responsible for a regionally pervasive and intense S_2–L_2 fabric and small-scale isoclines throughout the West Kaoko Zone and Central Kaoko Zone. D_2 fabrics including shallow NNW-plunging stretching lineations formed in a non-coaxial shear environment with highly constrictional strain during sinistral transpression in a wide mobile zone (Fig. A2) (Dürr and Dingeldey, 1996; Dingeldey, 1997). D_2 progresses continuously through D_3 intermediate folding events to D_4. WNW-plunging biotite and hornblende mineral lineations (L_4) develop (Fig. A2) associated with D_4 shortening by W over E over-folding producing the large-scale folds that dominate the Kaoko Belt (Fig. A1). D_2–D_3 and D_4 deformational episodes have tectonic transport directions at high angles to each other (Fig. A2). Later deformation events are insignificant and involved limited N–S shortening and formation of rare conjugate kink bands and E–W-trending upright folds (D_5). The Kaoko Belt was exhumed by passive uplift and erosion, without further compressional orogenesis and a later period of limited extension (rare normal faults and dolerite dykes) during the Cretaceous break up of South America and Africa.

A.2. Boudinage

There are two clearly recognisable episodes of boudinage in the Kaoko Belt, D_2–D_3 and D_4, with approximately orthogonal extension axes. 88% of all boudins investigated are D_2–D_3 boudins and are clearly related to formation of the pervasive and penetrative S_2–L_2 fabric. Nearly all boudin trains (with the exception of those described in Section 5.2) are parallel to the main foliations (foliation-parallel boudin trains). L_b is symmetrically distributed around L_2 for each boudin type with an orthogonal mean orientation. Therefore D_2–D_3 boudin extension axes (L_e), defined as the line normal to L_b within S_e, coincide with the L_2 stretching lineation (Fig. A2) and this is consistent with monoclinic boudin symmetry.

D_4 boudins have L_b at high angles to the sub-horizontal D_4 shortening axis associated with W over E over-folding (F_4) and boudin extension axes (L_e) are sub-parallel to L_4 mineral lineations (Fig. A2). F_4 fold axes are sub-parallel to L_2 and therefore D_4 boudin extension axes are at high angles to those developed during D_2 and form a distinct orientation population (Fig. A2). D_4 boudins form in two distinct scenarios: on the long limbs of F_4 folds, where the D_4 main foliation is sub-parallel to layering (i.e. foliation-parallel boudin trains) and in over-turned limbs, where layering is steeper than the D_4 main foliation and therefore foliation-oblique boudin trains form.

References

Berthé, D., Choukroune, P., Jegouzo, P., 1979. Orthogneiss, mylonite and non-coaxial deformation of granites: the example of the South Armorican shear zone. Journal of Structural Geology 1, 31–42.

Cloos, H., 1947. Boudinage. Transactions of the American Geophysical Union 28, 626–632.

Dingeldey, P., 1997. Tectono-Metamorphic Evolution of the Pan-African Kaoko Belt, NW-Namibia. Ph.D. Thesis, Würzburg University, Germany.

Dürr, S.B., Dingeldey, D.P., 1996. The Kaoko belt (Namibia): part of a late Neoproterozoic continental-scale strike-slip system. Geology 24, 505–506.

Etchecopar, A., 1974. Simulation par ordinateur de la deformation progressive d'un aggregat polycrystallin. Etude du development de structures orientees par ecrasement et cisaillement. Ph.D. thesis, Univerity of Nantes, France.

Etchecopar, A., 1977. A plane kinematic model of progressive deformation in a polycrystalline aggregate. Tectonophysics 39, 121–139.

Gaudemer, Y., Taponnier, P., 1987. Ductile and brittle deformations in the

northern Snake Range, Nevada. Journal of Structural Geology 9, 159–180.

Ghosh, S.K., Ramberg, H., 1976. Reorientation of inclusions by combination of pure and simple shear. Tectonophysics 34, 1–70.

Goldstein, A.G., 1988. Factors affecting the kinematic interpretation of asymmetric boudinage in shear zones. Journal of Structural Geology 10, 707–715.

Goscombe, B., 1991. Intense non-coaxial shear and the development of mega-scale sheath folds in the Arunta Block, Central Australia. Journal of Structural Geology 13, 299–318.

Goscombe, B., 1992. High-grade reworking of central Australian granulites. Part 1. Structural evolution. Tectonophysics 204, 361–399.

Goscombe, B., Everard, J.L., 2001. Tectonic evolution of Macquarie Island: extensional structures and block rotations in oceanic crust. Journal of Structural Geology 23, 639–673.

Goscombe, B., Passchier, C., 2001. Boudin trains as a kinematic tool kit. Geological Society of Australia, Abstracts 64, 63.

Grasemann, B., Stüwe, K., 2001. The development of flanking folds during simple shear and their use as kinematic indicators. Journal of Structural Geology 23, 715–724.

Hanmer, S.K., 1984. The potential use of planar and elliptical structures as indicators of strain regime and kinematics of tectonic flow. Current Research, Part B, Geological Survey of Canada, Paper 84-1B, pp. 133–142.

Hanmer, S., 1986. Asymmetrical pull-aparts and foliation fish as kinematic indicators. Journal of Structural Geology 8, 111–122.

Hanmer, S., Passchier, C., 1991. Shear-sense indicators: a review. Geological Survey of Canada. Paper 90-17, p. 72.

Hudleston, P.J., 1989. The association of folds and veins in shear zones. Journal of Structural Geology 11, 949–957.

Jordan, P.G., 1991. Development of asymmetric shale pull-aparts in evaporite shear zones. Journal of Structural Geology 13, 399–409.

Kröner, A., 1982. Rb–Sr geochronology and tectonic evolution of the Pan-African belt of Namibia. American Journal of Science 282, 1471–1507.

Lacassin, R., 1988. Large-scale foliation boudinage in gneisses. Journal of Structural Geology 10, 643–647.

Lister, G.S., Snoke, A.W., 1984. *S–C* mylonites. Journal of Structural Geology 6, 617–638.

Lloyd, G.E., Ferguson, C.C., Reading, K., 1982. A stress-transfer model for the development of extension fracture boudinage. Journal of Structural Geology 4, 355–372.

Malavieille, J., 1987. Kinematics of compressional and extensional ductile shearing deformation in a metamorphic core complex of the northeastern Basin and Range. Journal of Structural Geology 9, 541–554.

Malavieille, J., Lacassin, R., 1988. Bone-shaped boudins in progressive shearing. Journal of Structural Geology 10, 335–345.

Malavieille, J., Ritz, J.F., 1989. Mylonitic deformation of evaporites in décollements: examples from the Southern Alps, France. Journal of Structural Geology 11, 583–590.

Mandal, N., Karmakar, S., 1989. Boudinage in homogeneous foliation rocks. Tectonophysics 170, 151–158.

Mandal, N., Khan, D., 1991. Rotation, offset and separation of oblique-fracture (rhombic) boudins: theory and experiments under layer-normal compression. Journal of Structural Geology 13, 349–356.

Mandal, N., Chakraborty, C., Kamanta, S.K., 2000. Boudinage in multilayered rocks under layer-normal compression: a theoretical analysis. Journal of Structural Geology 22, 373–382.

Marcoux, J., Brun, J.-P., Ricou, L.E., 1987. Shear structures in anhydrite at the base of thrust sheets (Antalya, southern Turkey). Journal of Structural Geology 9, 555–561.

Mawer, C.K., 1987. Shear criteria in the Grenville Province, Canada. Journal of Structural Geology 9, 531–539.

McLellan, E.L., 1988. Migmatite structures in the Central Gneiss Complex, Boca de Quadra, Alaska. Journal of Metamorphic Geology 6, 517–542.

McNicoll, V.J., Brown, R.L., 1995. The Monashee décollement at Cariboo Alp, southern flank of the Monashee complex, southern British Columbia, Canada. Journal of Structural Geology 17, 17–30.

Means, W.D., Hobbs, B.E., Lister, G.S., Williams, P.F., 1980. Vorticity and non-coaxiality in progressive deformations. Journal of Structural Geology 2, 371–378.

Miller, R.Mc.G., Burger, A.J., 1983. U–Pb zircon age of the early Damaran Naauwpoort Formation. Special Publication of the Geological Society of South Africa 11, 267–272.

Passchier, C.W., 1987. Stable positions of rigid objects in non-coaxial flow: a study in vorticity analysis. Journal of Structural Geology 9, 679–690.

Passchier, C.W., 1997. The fabric attractor. Journal of Structural Geology 19, 113–127.

Passchier, C.W., 1998. Monoclinic model shear zones. Journal of Structural Geology 20, 1121–1137.

Passchier, C.W., 2001. Flanking structures. Journal of Structural Geology 23, 951–962.

Passchier, C.W., Simpson, C., 1986. Porphyroclast systems as kinematic indicators. Journal of Structural Geology 8, 831–843.

Passchier, C.W., Trouw, R.A.J., 1996. Microtectonics. Springer Verlag, Heidelberg.

Passchier, C.W., Druguet E., 2002. Numerical modelling of asymmetric boudinage. Journal of Structural Geology, 24, 1789–1803.

Platt, J.P., Vissers, R.L.M., 1980. Extensional structures in anisotropic rocks. Journal of Structural Geology 2, 397–410.

Ramberg, H., 1955. Natural and experimental boudinage and pinch-and-swell structures. Journal of Geology 63, 512–526.

Rast, N., 1956. The origin and significance of boudinage. Geological Magazine 93, 401–408.

Seth, B., Kroner, A., Mezger, K., Nemchin, A.A., Pidgeon, R.T., Okrusch, M., 1998. Archaean to Neoproterozoic magmatic events in the Kaoko belt of NW Namibia and their geodynamic significance. Precambrian Research 92, 341–363.

Simpson, C., 1984. Borrego Springs–Santa Rosa mylonite zone: a Late Cretaceous west-directed thrust in southern California. Geology 12, 8–11.

Simpson, C., Schmid, S.M., 1983. An evaluation of criteria to deduce the sense of movement in sheared rocks. Bulletin of the Geological Society of America 94, 1281–1288.

Stock, P., 1989. Zur antithetischen Rotation der Schieferung in Scherbandgefügen—ein kinematisches Deformationsmodell mit Beispielen aus der südlichen Gurktaler Decke. Frankfurter Geowissenschaftliche Arbeiten A7, 1–155.

Strömgård, K.E., 1973. Stress distribution during deformation of boudinage and pressure shadows. Tectonophysics 16, 215–248.

Swanson, M.T., 1992. Late Acadian–Alleghenian transpressional deformation: evidence from asymmetric boudinage in the Casco Bay area, coastal Maine. Journal of Structural Geology 14, 323–341.

Tvergaard, V., Needleman, A., Lo, K.K., 1981. Flow localisation in the plane strain tensile test. Journal of Mechanics and Physics of Solids 29, 115–142.

Uemura, T., 1965. Tectonic analysis of the boudin structure in the Muro group, Ku Peninsula, Southwest Japan. Journal of Earth Sciences 13, 99–114.

Waldron, J.W.F., Turner, D., Stevens, K.M., 1988. Stratal disruption and development of mélange, Western Newfoundland: effect of high fluid pressure in an accretionary terrain during ophiolite emplacement. Journal of Structural Geology 10, 861–873.

Yamamoto, H., 1994. Kinematics of mylonitic rocks along the Median Tectonic Line, Akaishi Range, central Japan. Journal of Structural Geology 16, 61–70.